







BRIEF DEFINITIVE REPORT

Essential cell-extrinsic requirement for PDIA6 in lymphoid and myeloid development

Jin Huk Choi^{1,2} , Xue Zhong¹, Zhao Zhang¹, Lijing Su¹, William McAlpine¹ , Takuma Misawa¹, Tzu-Chieh Liao¹, Xiaoming Zhan¹, Jamie Russell¹ , Sara Ludwig¹, Xiaohong Li¹, Miao Tang¹, Priscilla Anderton¹ , Eva Marie Y. Moresco¹ , and Bruce Beutler¹ 

In a forward genetic screen of N-ethyl-N-nitrosourea (ENU)-induced mutant mice for aberrant immune function, we identified mice with a syndromic disorder marked by growth retardation, diabetes, premature death, and severe lymphoid and myeloid hypoplasia together with diminished T cell-independent (TI) antibody responses. The causative mutation was in *Pdia6*, an essential gene encoding protein disulfide isomerase A6 (PDIA6), an oxidoreductase that functions in nascent protein folding in the endoplasmic reticulum. The immune deficiency caused by the *Pdia6* mutation was, with the exception of a residual T cell developmental defect, completely rescued in irradiated wild-type recipients of PDIA6-deficient bone marrow cells, both in the absence or presence of competition. The viable hypomorphic allele uncovered in these studies reveals an essential role for PDIA6 in hematopoiesis, but one extrinsic to cells of the hematopoietic lineage. We show evidence that this role is in the proper folding of Wnt3a, BAFF, IL-7, and perhaps other factors produced by the extra-hematopoietic compartment that contribute to the development and lineage commitment of hematopoietic cells.

Introduction

Lifelong generation of blood and immune cells from hematopoietic stem cells (HSCs) depends on the organized expression of lineage-specific transcriptional programs, and extrinsic regulation through cellular or molecular components of the microenvironment that support homeostasis of HSCs and immune cells (Osawa et al., 1996; Sawai et al., 2016). While many of the transcription factors that dictate lineage commitment are known, extra-hematopoietic factors that contribute to the maintenance of HSCs and lymphoid/myeloid survival have only begun to be elucidated (Anthony and Link, 2014; Lee et al., 2017).

Protein disulfide isomerase A6 (PDIA6), also known as ER protein 5 (P5 or ERP5), is an oxidoreductase that exhibits enzymatic properties similar to other protein disulfide isomerases (PDIs), catalyzing oxidation, reduction, and isomerization of disulfide bonds during nascent protein folding (Kikuchi et al., 2002; Laurindo et al., 2012). PDIA6 functions as an attenuator of the unfolded protein response by inhibiting aggregation of misfolded proteins in the ER (Eletto et al., 2014). Furthermore, at the cell surface, PDIA6 physically associates with the integrin β_3 subunit to promote platelet activation after stimulation (Jordan et al., 2005; Passam et al., 2015). Although its enzymatic role in protein folding has been extensively studied, the physiological requirements for PDIA6 in vivo have remained largely obscure.

In this study, we observed that PDIA6 is critical for organism survival, growth, and insulin biosynthesis, as well as for the development of HSCs and all lymphoid/myeloid lineages in mice. In this latter role, the critical function of PDIA6 is exercised chiefly in the extra-hematopoietic compartment.

Results and discussion

To identify novel regulators of adaptive immunity and/or metabolism, we performed a forward genetic screen in mice carrying N-ethyl-N-nitrosourea (ENU)-induced mutations. Among the phenovariants discovered, several mice from a single pedigree exhibited reduced body weights (Fig. 1 A) and diminished T cell-independent (TI) antibody responses to NP-Ficoll compared with WT littermates (Fig. 1 B). The mice also exhibited moderately decreased T cell-dependent antibody responses to aluminum hydroxide (alum)-precipitated OVA (OVA/alum; Fig. 1 C). The phenotype, named *braum*, was transmitted as a recessive trait. By pedigree mapping, the *braum* phenotype was correlated with a mutation in *Pdia6* (Fig. 1 D). The *braum* mutation, present in the affected pedigree, resulted in a valine (V) to alanine (A) substitution at position 32 (V32A) in the first thioredoxin domain of the PDIA6 protein (Fig. 1 E), which was

¹Center for the Genetics of Host Defense, University of Texas Southwestern Medical Center, Dallas, TX; ²Department of Immunology, University of Texas Southwestern Medical Center, Dallas, TX.

Correspondence to Bruce Beutler: Bruce.Beutler@UTSouthwestern.edu.

© 2020 Choi et al. This article is distributed under the terms of an Attribution-Noncommercial-Share Alike-No Mirror Sites license for the first six months after the publication date (see <http://www.rupress.org/terms/>). After six months it is available under a Creative Commons License (Attribution-Noncommercial-Share Alike 4.0 International license, as described at <https://creativecommons.org/licenses/by-nc-sa/4.0/>).

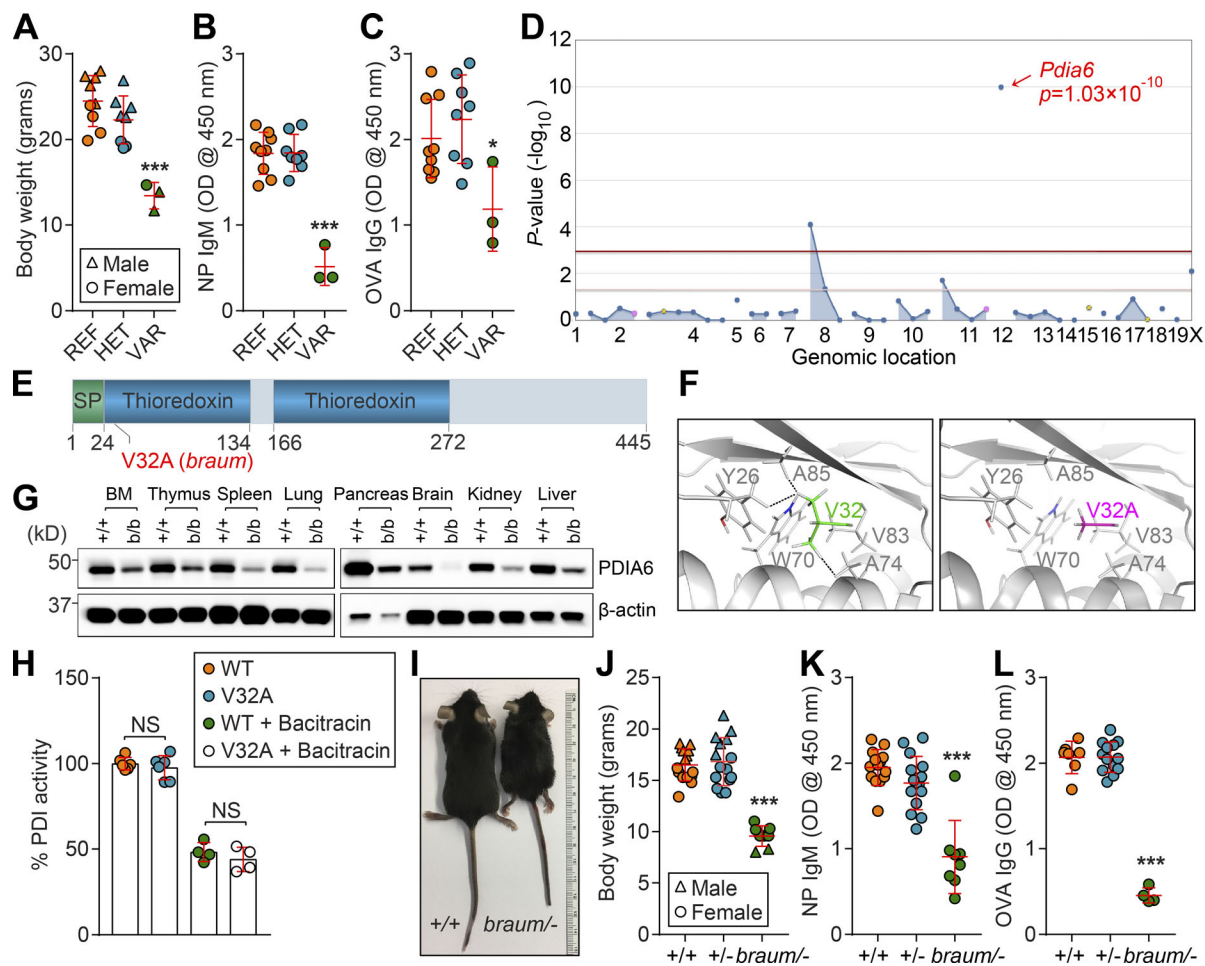


Figure 1. The *braum* phenotype. (A) Body weights of 12-wk-old *braum* mice and WT littermates ($n = 3$ –9 mice/genotype). (B and C) T1 (B) and T cell-dependent (C) antibody responses after immunization with NP-Ficoll and OVA/alum, respectively, in 12-wk-old *braum* mice and WT littermates ($n = 3$ –9 mice/genotype). Data presented as absorbance at 450 nm. (D) Manhattan plot showing P values for linkage of the body weight phenotype to mutations in the *braum* pedigree calculated using a recessive model of inheritance. The $-\log_{10}$ P values (y axis) are plotted vs. the chromosomal positions of mutations (x axis) identified in the affected pedigree. Horizontal red or pink lines represent thresholds of $P = 0.05$ with or without Bonferroni correction, respectively. (E) Protein domains of mouse PDIA6 (445 aa in length). The location of the *braum* mutation, which results in V32A in PDIA6, is highlighted in red. (F) Enlarged view of the hydrophobic pocket surrounding V32 of mouse PDIA6 (PDB ID: 2DML). The side chains of the hydrophobic residues are shown in sticks. Left panel: The V32 side chain (green) makes hydrophobic contacts (dashed lines) with the surrounding residue side chains, especially A85, Y26, and A74. Right panel: V32 mutated to A (magenta) using the PyMol mutagenesis function. (G) PDIA6 expression in tissue lysates from 10-wk-old *braum* homozygotes and WT littermates. (H) The catalytic reduction of insulin in the presence of dithiothreitol by WT and mutant (V32A) PDIA6 proteins determined by fluorescence-based assay ($n = 4$ –6 samples/group). Data are normalized to PDI activity of WT PDIA6. (I and J) Photograph of male *braum*^{-/-} mouse (I) and body weight (J) of *braum*^{-/-} and WT littermates at 12 wk of age ($n = 8$ –15 mice/genotype). (K and L) T1 (K) and T cell-dependent (L) antibody responses after immunization with NP-Ficoll and OVA/alum, respectively, in 10-wk-old *braum*^{-/-} mice and littermates with indicated genotype ($n = 4$ –15 mice/group). Data presented as absorbance at 450 nm. Data points represent individual mice (A–C and J–L). P values were determined by one-way ANOVA with Dunnett's multiple comparisons test (A–C, H, and J–L). Data are representative of one (A–C, G, and J) or two independent experiments (H, K, and L). Error bars indicate SD. *, $P < 0.05$; ***, $P < 0.001$. REF, homozygous for C57BL/6J *Pdia6* reference allele; HET, heterozygous for *Pdia6* reference allele and *braum* allele; VAR, homozygous for *Pdia6 braum* allele; SP, signal peptide.

predicted to be damaging by PolyPhen-2 (score = 1.000; Adzhubei et al., 2010). We examined the structural effect of the *braum* mutation by modeling a V32A mutation in PDIA6 (PDB ID: 2DML) using PyMol2.2 software. Analysis of the hydrophobic pocket surrounding V32 in mouse PDIA6 showed hydrophobic contacts between V32 and the side chains of A85, Y26, and A74 (Fig. 1 F, left). However, when V32 was mutated to an A (V32A), the distances between the mutated A32 and A85/Y26/A74 increased (Fig. 1 F, right), which is predicted to impair hydrophobic interactions and induce conformational changes impacting protein function. Immunoblotting showed that PDIA6 is widely expressed

throughout the body. Decreased levels of PDIA6 protein were detected in mice carrying the V32A mutation compared with WT littermates, suggesting that the *braum* mutation impairs protein stability (Fig. 1 G). However, the mutant PDIA6 protein was found to possess isomerase activity at an average level ~97% of that measured for the molar equivalent of the WT PDIA6 protein (Fig. 1 H).

To date, PDIA6-deficient or -mutant mice have not been phenotypically characterized. A CRISPR/Cas9 knockout allele of *Pdia6* yielded no homozygous pups, leading us to conclude that complete ablation of this gene causes prenatal lethality

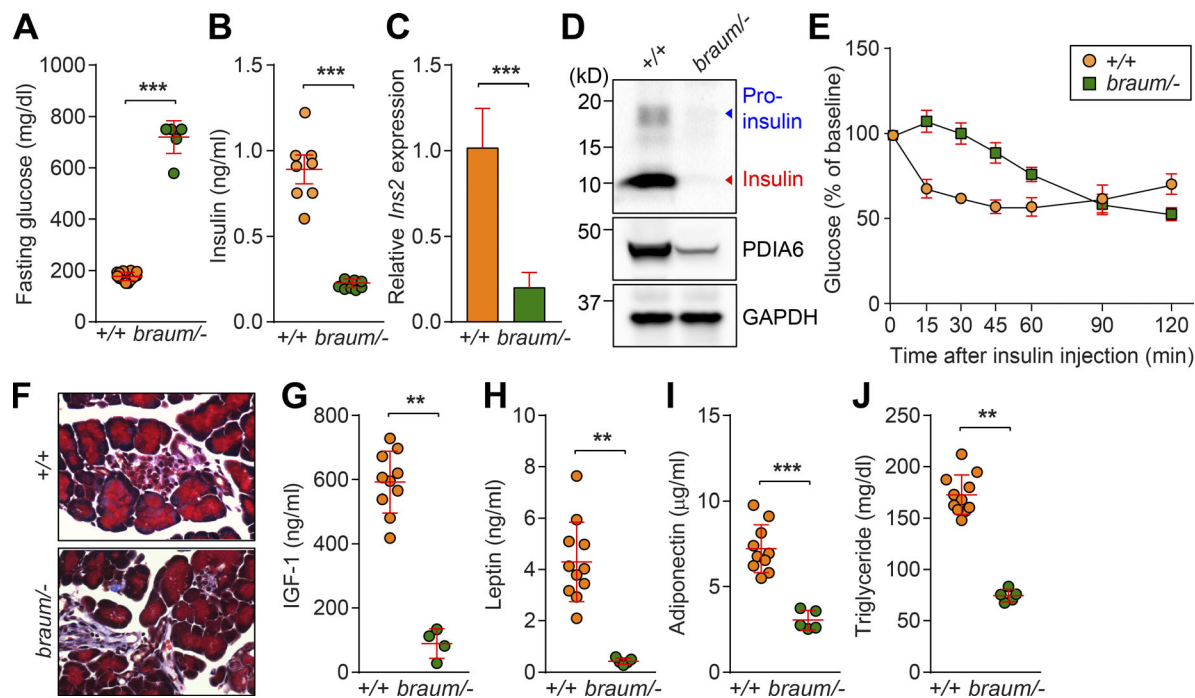


Figure 2. Altered glucose metabolism caused by a *Pdia6* mutation in mice. (A, B, and G–J) Serum glucose (A), insulin (B), IGF-1 (G), leptin (H), adiponectin (I), and triglyceride (J) in 12-wk-old mice after a 6-h fast ($n = 4$ –16 mice/genotype). **(C)** *Ins2* transcript levels normalized to *Gapdh* mRNA in pancreases of *braum*^{-/-} mice and WT littermates at 12 wk of age ($n = 3$ –5 mice/genotype). **(D)** Lysates of pancreases isolated from 12-wk-old *braum*^{-/-} mice and WT littermates were immunoblotted using antibodies against insulin and PDIA6. GAPDH was used as a loading control. **(E)** Insulin tolerance test. Blood glucose was measured at the indicated times after i.p. insulin injection in 12-wk-old mice ($n = 5$ –7 mice/genotype). **(F)** Representative hematoxylin and eosin staining of *braum*^{-/-} and WT littermate pancreases at 12 wk of age ($n = 3$ mice/genotype). Data points represent individual mice (A, B, and G–J). P values were determined by Student's *t* test. Data are representative of one (E) or two independent experiments (A–D and F–J). Error bars indicate SD. **, $P < 0.01$; ***, $P < 0.001$.

($P < 0.0001$; χ^2 test; $n = 62$ mice: 20 *Pdia6*^{+/+}, 42 *Pdia6*^{+/-}). We then crossed *braum* heterozygotes (*Pdia6*^{*braum*/+}) with CRISPR/Cas9-targeted *Pdia6* heterozygotes (*Pdia6*^{+/-}), which were phenotypically normal in both cases, to generate *Pdia6* compound heterozygotes (*Pdia6*^{*braum*/-}; hereafter *braum*^{-/-}) with simple heterozygosity for all residual ENU-induced mutations. Offspring with the *braum*^{-/-} genotype were born at expected Mendelian frequencies ($P = 0.50$, χ^2 test; $n = 104$ mice: 31 *Pdia6*^{+/+}, 53 *Pdia6*^{+/-} or *Pdia6*^{*braum*/+}, 20 *Pdia6*^{*braum*/-}). The *braum*^{-/-} mice showed reduced body sizes and weights (Fig. 1, I and J, respectively), and diminished TI and T cell-dependent antibody responses to NP-Ficoll and OVA/alum immunization (Fig. 1, K and L, respectively) compared with WT littermates, conclusively establishing the hypomorphic nature of the *Pdia6*^{*braum*} mutation and its causative relationship with the observed phenotype in *braum*^{-/-} mice.

Significantly elevated fasting blood glucose levels were detected in the *braum*^{-/-} mice as early as 4–6 wk of age (Fig. 2 A); thereafter, the hyperglycemia persisted and *braum*^{-/-} mice died by 3–4 mo of age. We found that the *braum*^{-/-} mice had significantly lower serum insulin concentrations compared with WT littermates (Fig. 2 B). Misfolded proinsulin is a putative PDIA6 substrate during ER-associated degradation (Gorasia et al., 2016), and silencing of PDIA6 in cell lines disinhibited the endonuclease activity of IRE-1 toward insulin transcripts (Eletto et al., 2016). Consistent with the latter finding, we confirmed a dramatic decrease in *Ins2* mRNA and pro-/mature-insulin levels

in the *braum*^{-/-} pancreas by quantitative PCR and immunoblot, respectively (Fig. 2, C and D). Similar to a model of type 1 diabetes, the nonobese diabetic mouse (Makino et al., 1980), we found that *braum*^{-/-} mice showed insulin resistance compared with WT littermates in insulin tolerance tests (Fig. 2 E). However, pancreases from *braum*^{-/-} mice did not show marked histopathological changes in islet architecture compared with those from WT littermates (Fig. 2 F). Furthermore, decreased amounts of IGF-1 (Fig. 2 G), adipokines (Fig. 2, H and I), and triglycerides (Fig. 2 J) were detected in *braum*^{-/-} serum. These data demonstrate that altered glucose metabolism, insulin biosynthesis, and adaptive immune responses all result from reduced function of PDIA6 in mice.

To further characterize the immunological defect caused by the *Pdia6* mutation, we immunophenotyped mice by complete blood cell count testing and flow cytometry analysis of lymphoid and myeloid cells in blood and spleen. The *braum*^{-/-} mice had reduced numbers of white blood cells, lymphocytes, monocytes, and platelets; neutrophil numbers were normal (Fig. 3 A). Gross examination of lymphoid organs showed that, unlike young *braum*^{-/-} mice, adult *braum*^{-/-} mice had hypoplastic thymi and spleens (Fig. 3 B). Quantitation of cell numbers (Fig. 3 C) and flow cytometry analysis of blood cells (Fig. 3 D) showed that cytopenia in the *braum*^{-/-} mice was age-dependent and progressed after 6 wk of age. In addition, the frequencies of natural killer (NK) and NK1.1⁺ T cells (Fig. 3 E) were significantly reduced in *braum*^{-/-} mice compared with WT littermates. The

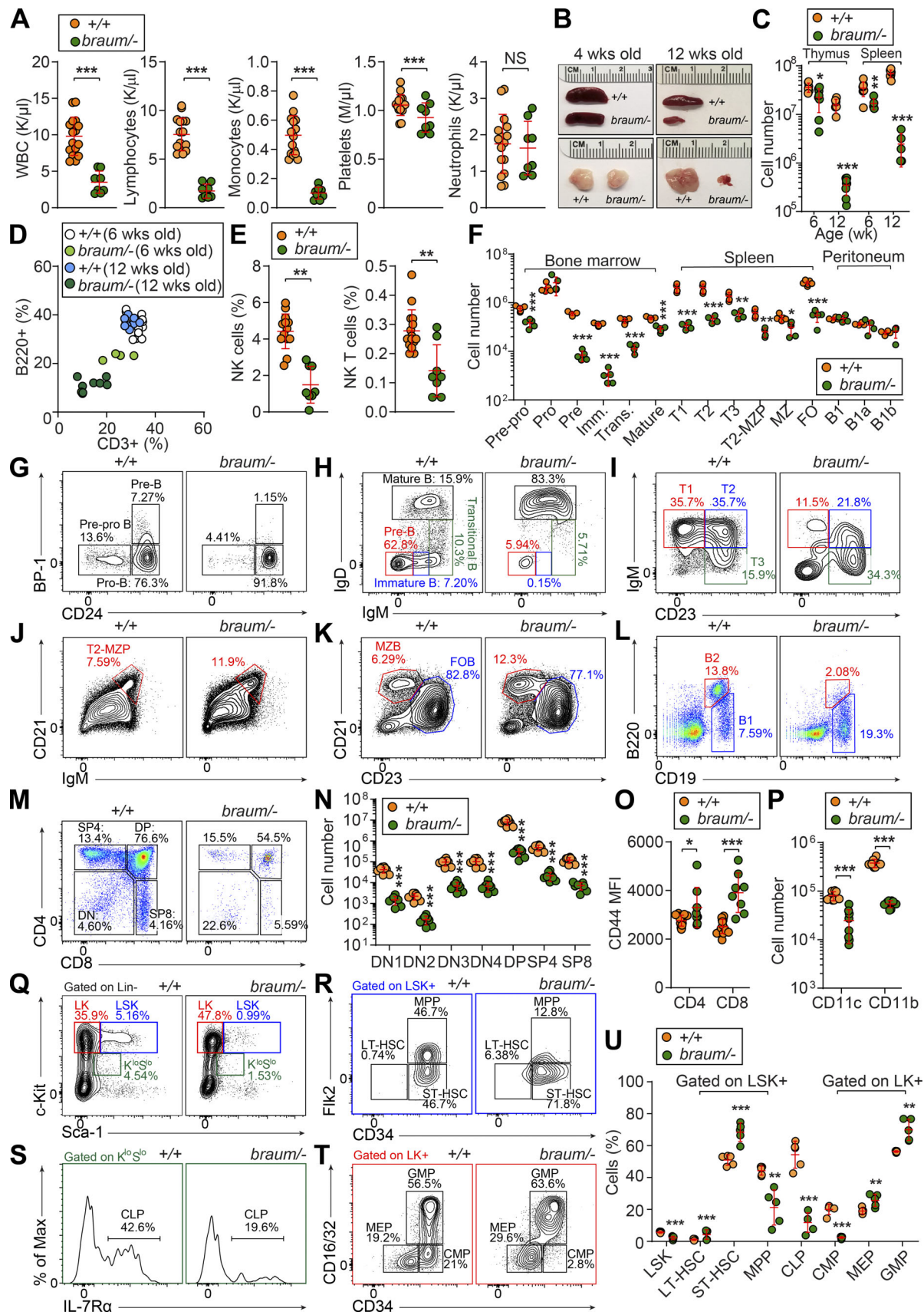


Figure 3. **Severe immune deficiency caused by a *Pdia6* mutation in mice.** (A) Whole blood cell counts of white blood cells, lymphocytes, monocytes, platelets, and neutrophils in 12-wk-old *braum*^{-/-} and WT littermates (*n* = 8–16 mice/genotype). (B) Representative photographs of spleen and thymus isolated

from 4- or 12-wk-old *braum*^{-/-} and WT littermates. **(C)** Thymocyte and splenocyte counts from 6- or 12-wk-old *braum*^{-/-} and WT littermates (*n* = 5–8 mice/genotype). **(D)** Frequency of B220⁺ cells plotted versus frequency of CD3⁺ T cells in peripheral blood from 6- or 12-wk-old *braum*^{-/-} and WT littermates (*n* = 4–14 mice/group). **(E)** Frequency of peripheral blood NK and NK1.1⁺ T cells from 12-wk-old *braum*^{-/-} and WT littermates (*n* = 8–15 mice/genotype). **(F)** Numbers of B cell subsets in bone marrow, spleen, and peritoneal cavity of 12-wk-old *braum*^{-/-} and WT littermates (*n* = 4–7 mice/genotype). **(G–L)** Representative flow cytometry plots showing B cell development in the bone marrow (G and H), spleen (I–K), and peritoneal cavity (L) from 12-wk-old *braum*^{-/-} and WT littermates. Each B cell subset was gated as follows: pre-pro B: B220^{low}BP-1⁺CD24^{low}, pro-B: B220^{low}BP-1⁺CD24⁺, immature B (Imm.): B220⁺IgM⁺IgD⁻, transitional B (Trans.): B220⁺IgM^{high}IgD^{low}, mature recirculating B: B220⁺IgD⁺IgM⁺, T1: B220⁺CD93⁺IgM^{high}CD23⁻, T2: B220⁺CD93⁺IgM^{high}CD23⁺, marginal zone precursor (MZP): B220⁺CD93⁺IgM⁺CD21⁺CD23^{high}, T3: B220⁺CD93⁺IgM^{low}CD23⁺, follicular B (FOB): B220⁺CD93⁺IgM⁺CD21⁺CD23^{high}, marginal zone B (MZB): B220⁺CD93⁺IgM⁺CD21⁺CD23^{low}, B2: B220⁺CD19⁺, B1: B220^{low}CD19⁺ (*n* = 4–7 mice/genotype). **(M and N)** Percentages (M) and numbers (N) of thymocytes in 12-wk-old *braum*^{-/-} and WT littermates (*n* = 8 mice/genotype). **(O)** Flow-cytometry analysis of CD44 expression (mean fluorescence intensity, MFI) on splenic CD4⁺ and CD8⁺ T cells in 12-wk-old *braum*^{-/-} and WT littermates (*n* = 8–15 mice/genotype). **(P)** Numbers of CD11c⁺ and CD11b⁺ myeloid cells in the spleen of 12-wk-old *braum*^{-/-} and WT littermates (*n* = 8 mice/genotype). **(Q–U)** Representative flow cytometry plots (Q–T) and quantitative analysis (U) of the HSC and progenitor populations in the bone marrow of *braum*^{-/-} and WT littermates (*n* = 5 mice/genotype). Data points represent individual mice (A, C–F, N–P, and U). P values were determined by Student's *t* test. Numbers adjacent to outlined areas or in quadrants indicate percent cells in each (G–M and Q–T). Data are representative of three independent experiments (A–U). Error bars indicate SD. *, *P* < 0.05; **, *P* < 0.01; ***, *P* < 0.001. CLP, common lymphoid progenitor; CMP, common myeloid progenitor; GMP, granulocyte-macrophage progenitor; LT, long-term; MEP, megakaryocyte-erythrocyte progenitor; MPP, multipotent progenitor; ST, short-term.

braum^{-/-} mice had reduced numbers of B cell progenitors in the bone marrow beginning at the prepro-B stage, a defect in the pro-B to pre-B transition, and very few cells progressed to the immature B stage (Fig. 3, F and G). Although the frequency of mature recirculating B cells in the bone marrow appeared increased in *braum*^{-/-} mice compared with WT littermates (Fig. 3 H), the total numbers were decreased (Fig. 3 F). In the spleen, *braum*^{-/-} mice had one tenth the normal number of B220⁺ cells, largely due to a lack of transitional and follicular B cell subsets (Fig. 3, F, I, and K). The frequencies of marginal zone precursors and marginal zone B cells in the spleen appeared increased in *braum*^{-/-} mice compared with WT littermates, but the total numbers were also decreased (Fig. 3, F, J, and K). However, the total number of B-1 cells in the peritoneal cavity was not affected in *braum*^{-/-} mice compared with WT littermates (Fig. 3, F and L). The *braum*^{-/-} mice had abnormal frequencies of thymocyte subsets as indicated by increased double negative cells with a concomitant decrease in double positive cells compared with WT littermates (Fig. 3 M); however, total numbers of each subset were significantly decreased (Fig. 3 N). The expression of surface glycoprotein CD44 was increased in *braum*^{-/-} mice compared with WT littermates (Fig. 3 O). Furthermore, *braum*^{-/-} mice had significantly fewer CD11c⁺ or CD11b⁺ myeloid cells compared with WT mice (Fig. 3 P). Collectively, these data demonstrate that PDIA6 is essential for lymphoid and myeloid development.

Lymphocytes and myeloid cells originate from hematopoietic stem and progenitor cells in the bone marrow. Since the *braum*^{-/-} mice exhibited both lymphoid and myeloid development defects, we suspected a fault in the hematopoietic stem and progenitor cells. We found a decrease in the proportion of LSK⁺ cells in the *braum*^{-/-} mice (Fig. 3, Q and U). The composition of the LSK⁺ compartment was significantly altered in *braum*^{-/-} bone marrow, resulting in a reduction in multipotent progenitors and a concomitant increase in long-term and short-term HSCs compared with WT mice (Fig. 3, R and U). A significant reduction in common lymphoid progenitors was also observed in the *braum*^{-/-} mice (Fig. 3, S and U). In addition, *braum*^{-/-} bone marrow showed altered LK⁺ cell composition caused by a reduction in common myeloid progenitors and an increase in megakaryocyte-erythrocyte

progenitors and granulocyte-macrophage progenitors (Fig. 3, T and U). These findings suggest that PDIA6 deficiency affects hematopoietic cell development from early stages of commitment to hematopoietic lineages.

To distinguish between hematopoietic and extra-hematopoietic origins of the immune cell defects, we reconstituted irradiated WT (CD45.1) or *Rag2*^{-/-} (CD45.2) recipients with unmixed WT (CD45.2), *braum*^{-/-} (CD45.2), or a 1:1 mixture of *braum*^{-/-} (CD45.2) and WT (CD45.1) bone marrow cells. In the absence or presence of competition, bone marrow cells from *braum*^{-/-} mice repopulated B220⁺, NK, and CD11c⁺ myeloid cells in the spleen of irradiated recipients as efficiently as cells derived from WT donors (Fig. 4, A and B). The relative proportions of T cell pools in mixed chimeras showed that *braum*^{-/-}-derived cells were at a mild competitive disadvantage in repopulating SP4 and SP8 cells in the thymus and periphery compared with cells derived from WT donors (Fig. 4, C and D). In contrast to the B cell development defects observed in the bone marrow of *braum*^{-/-} mice (Fig. 3, G and H), *braum*^{-/-} B cell progenitors in the bone marrow of irradiated WT recipient mice showed substantial rescue of the pre-pro B > pro-B > pre-B transitions (Fig. 4 E). In addition, irradiated WT recipients reconstituted with *braum*^{-/-} bone marrow mounted TI antibody responses comparable to those of irradiated WT recipients engrafted with WT bone marrow (Fig. 4 F). These data indicate that the effects of reduced function of PDIA6 on lymphoid and myeloid development are non-cell-autonomous.

We also investigated effects of extra-hematopoietic PDIA6 function on T cell proliferation and homeostasis. To test this, we measured the OVA-induced proliferation of OVA-specific OT-II T cells transferred into either *braum*^{-/-} or WT littermates. In contrast to OT-II cells transferred to WT recipients, OT-II T cells transferred into *braum*^{-/-} hosts showed significant proliferation defects after OVA injection as measured by number of divisions and counts of OT-II cells that underwent proliferation in host spleen (Fig. 4 G and Fig. S1). To test whether a cell-intrinsic proliferation defect affected *braum*^{-/-} T cells, we measured in vivo T cell survival and proliferative responses of CellTrace Far Red dye-labeled WT or *braum*^{-/-} T cells injected into sublethally irradiated WT recipients. As a control, unirradiated

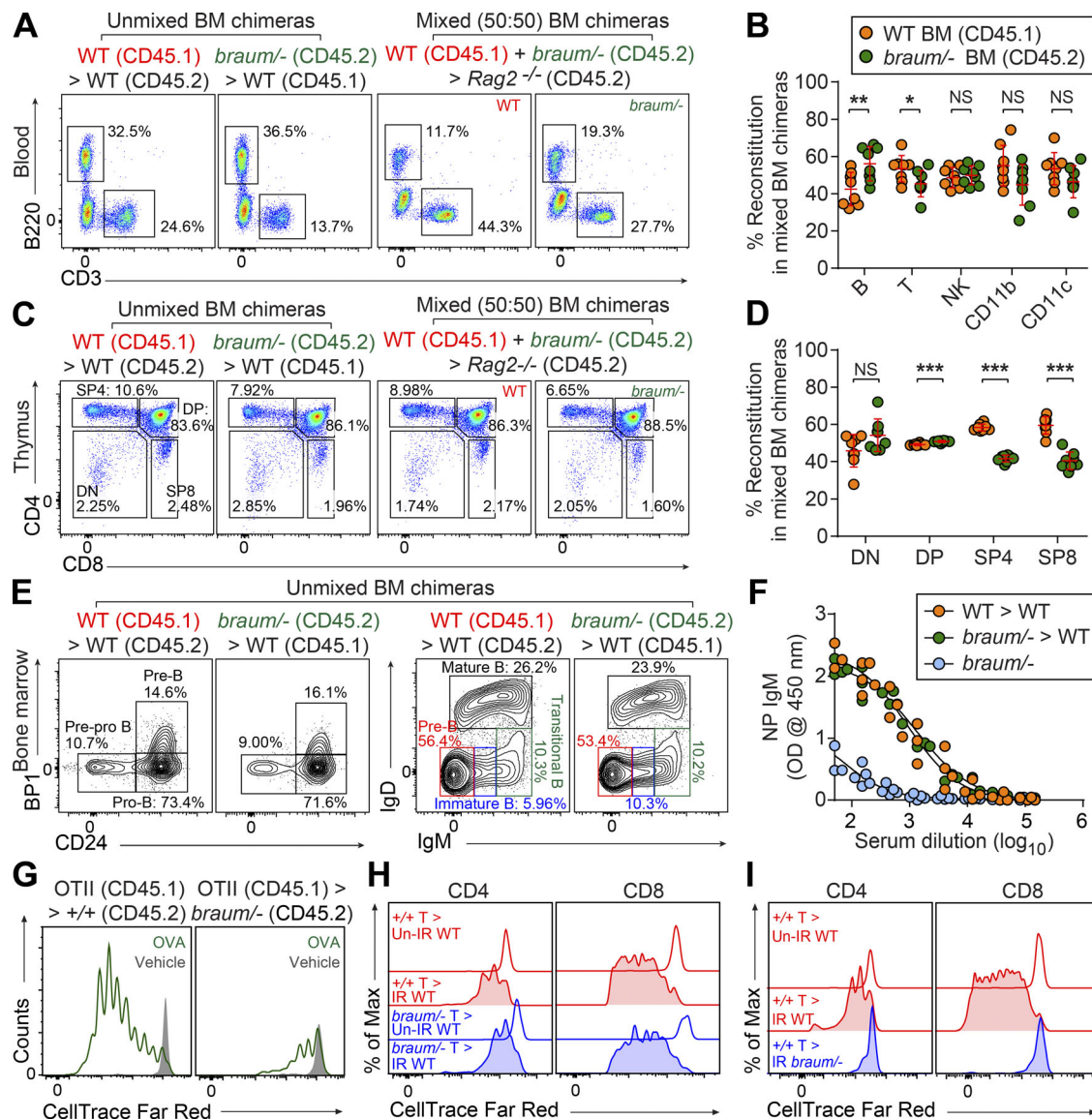


Figure 4. *Pdia6* mutant mice exhibit a cell-extrinsic failure of lymphocyte development. (A–E) Repopulation of lymphocytes in the blood (A and B), thymus (C and D), and bone marrow (E) 12 wk after reconstitution of irradiated WT mice (CD45.1 or CD45.2) with *braum*^{-/-} (CD45.2) or WT (C57BL/6J; CD45.1) bone marrow, or *Rag2*^{-/-} recipients with a 1:1 mixture of *braum*^{-/-} (CD45.2) and WT (CD45.1) bone marrow ($n = 8$ mice/genotype). Numbers adjacent to outlined areas or in quadrants (A, C, and E) indicate percent cells in each. (F) T1 antibody responses after immunization with NP-Ficoll in bone marrow chimeras 12 wk after reconstitution. 10-wk-old *braum*^{-/-} mice served as controls ($n = 4$ or 5 mice/genotype). Data presented as absorbance at 450 nm. (G) Impaired antigen-specific expansion of WT OT-II T cells in *braum*^{-/-} mice. CellTrace Far Red-labeled WT OT-II T cells (CD45.1) were adoptively transferred into WT (C57BL/6J; CD45.2) or *braum*^{-/-} (CD45.2) hosts ($n = 5$ mice/group). Representative flow-cytometry histogram of the CellTrace Far Red dilution in *braum*^{-/-} and WT littermates 72 h after injection of soluble OVA or sterile PBS (vehicle) as a control. (H and I) Impaired homeostatic expansion of WT T cells in *braum*^{-/-} mice. CellTrace Far Red-labeled WT or *braum*^{-/-} T cells were adoptively transferred into sub-lethally irradiated (IR; 8.5 Gy) *braum*^{-/-} or WT hosts ($n = 5$ mice/group). CellTrace Far Red dilution was analyzed in the spleens of recipients 6 d after adoptive transfer. Data points represent individual mice (B, D, and F). P values were determined by Student's *t* test. Numbers adjacent to outlined areas or in quadrants indicate percent cells in each (A, C, and E). Data are representative of two independent experiments (A–I). Error bars indicate SD. *, $P < 0.05$; **, $P < 0.01$; ***, $P < 0.001$. Max, maximum; DN, double negative (CD4⁻CD8⁻); DP, double positive (CD4⁺CD8⁺).

recipients were injected in an identical manner. Spleens were harvested 6 d after adoptive transfer and assessed for T cell proliferation. CD8⁺ and CD4⁺ *braum*^{-/-} donor T cells recovered from the irradiated recipients proliferated to a similar extent as WT donor cells (Fig. 4 H). In contrast, proliferation of WT donor T cells in spleens of irradiated *braum*^{-/-} recipients was significantly decreased compared with proliferation in irradiated WT

recipients (Fig. 4 I). Together, these findings demonstrate that *braum*^{-/-} T cells are intrinsically capable of proliferation but that T cell-extrinsic proliferation signals are impaired in *braum*^{-/-} mice.

Taking into account the known enzymatic function of PDIA6 and the metabolic and immune phenotypes observed in the *braum*^{-/-} mice, we hypothesized that PDIA6 regulates the folding of numerous proteins required for development, energy balance,

and hematopoiesis. In the immune system, PDIA6 might be directly involved in the folding of secretory proteins produced by extra-hematopoietic cells that play critical roles in the survival and homeostasis of immune cells. To test this hypothesis, we first examined whether PDIA6 might be necessary for the folding of Wnt3a, a cysteine-rich lipoprotein produced by stromal cells that regulates HSC self-renewal through activation of canonical and noncanonical Wnt signaling pathways (MacDonald et al., 2014; Reya et al., 2003; Sugimura et al., 2012). We used CRISPR/Cas9 to knock out *Pdia6* in L-Wnt3a cells that constitutively secrete Wnt3a protein. Reduced Wnt3a expression was detected in both total cell lysate and conditioned media from *Pdia6*^{-/-} cells compared with parental L-Wnt3a cells (Fig. 5 A), suggesting that PDIA6 is required for Wnt3a folding and subsequent secretion.

B cell development and homeostasis are supported by B cell-activating factor (BAFF) produced by stromal and various myeloid cells together with tonic signaling through the B cell receptor (Kraus et al., 2004; Mackay et al., 2003). It has been suggested that BAFF production by myeloid cells alone is not sufficient to support normal B cell survival, emphasizing the importance of BAFF production by extra-hematopoietic cells (e.g., stromal cells; Gorelik et al., 2003). Full-length BAFF contains three cysteine residues, two of which, Cys232 and Cys245 in β -strands E and F, respectively, form a disulfide bridge. A third cysteine residue (Cys146) is located at the N terminus of β -strand A and is not disulfide bonded (Chen et al., 2004; Karpusas et al., 2002). Consistent with previous reports, we confirmed that *Rag2*^{-/-} and *Ighm*^{-/-} mice, which lack B cells, had high serum BAFF levels (Fig. 5 B). Interestingly, we found that *braum*^{-/-} mice had comparable levels of serum BAFF to WT littermates, although they have severe B cell deficiency (Fig. 5 B). To examine if the extra-hematopoietic compartment of *braum*^{-/-} mice had BAFF production defects, we sublethally irradiated *braum*^{-/-} mice or WT littermates to induce transient lympho- and myelopenia. As expected, irradiation resulted in elevated serum BAFF levels in WT mice compared with unirradiated WT mice (Fig. 5 B). Irradiation also resulted in elevated serum BAFF levels in the *braum*^{-/-} mice compared with unirradiated *braum*^{-/-} mice; however, the level was significantly lower than that in irradiated WT mice (Fig. 5 B). In addition, significantly lower serum BAFF levels were detected in *braum*^{-/-}; *Rag2*^{-/-} mice compared with +/+; *Rag2*^{-/-} mice (Fig. 5 C). Expression of FLAG-tagged BAFF transiently transfected into *Pdia6*^{-/-} L-Wnt3a cells was reduced compared with that in similarly transfected parental L-Wnt3a cells (Fig. 5 D). These results provide evidence that mutation of PDIA6 significantly impairs BAFF production in the extra-hematopoietic compartment.

Homeostatic expansion cues delivered predominantly by cytokines IL-7 and IL-15 produced by stromal and thymic epithelial cells together with weak tonic signaling through the T cell receptor and self-MHC/peptide ligands are critical for T cell survival (Ernst et al., 1999; Tan et al., 2001). Besides its essential function in T cell development, IL-7 also plays a key role in the proliferation and survival of B cell progenitors during development (Corfe and Paige, 2012). Mature IL-7 and -15 contain cysteine residues (Cosenza et al., 1997; Fehniger and Caligiuri,

2001), and it has been reported that reduction with β -mercaptoethanol causes loss of IL-7/15 biological activity, suggesting that intramolecular disulfide bonds play a role in their activity (Henney, 1989). The T cell-extrinsic homeostatic proliferation defects observed in irradiated *braum*^{-/-} recipients (Fig. 4, H and I) suggest that reduced function of PDIA6 impairs secreted signals from stromal cells and/or thymic epithelial cells (Hara et al., 2012), possibly IL-7 or IL-15, by causing their misfolding. To test this hypothesis, we measured IL-7 levels in the bone marrow of *braum*^{-/-} mice. Consistent with elevated serum BAFF levels induced in irradiated mice (Fig. 5, B and C), irradiation resulted in elevated IL-7 levels in WT mice compared with unirradiated WT mice (Fig. 5 E). Although *braum*^{-/-} mice have severe lympho- and myelopenia (Fig. 2), unirradiated *braum*^{-/-} mice had IL-7 levels comparable to unirradiated WT mice (Fig. 5 E). However, IL-7 levels in irradiated *braum*^{-/-} mice were significantly lower than those in irradiated WT mice. Furthermore, transient transfection of *Pdia6*^{-/-} L-Wnt3a cells or their parental cells with a plasmid encoding FLAG-tagged IL-7 resulted in decreased levels of IL-7 expression in *Pdia6*^{-/-} cells compared with parental L-Wnt3a cells (Fig. 5 F). Together, these data support the idea that mutation of *Pdia6* results in impairments in the folding of IL-7, which is necessary for hematopoiesis.

Next, we investigated the effect of PDIA6 mutation on the bioactivity of BAFF and IL-7 in *braum*^{-/-} mice. We measured the proliferative response of CellTrace Far Red dye-labeled WT naive B cells (CD45.1) transferred into either unirradiated *braum*^{-/-} or WT littermates (CD45.2). In contrast to WT B cells transferred to WT recipients, the B cells transferred into *braum*^{-/-} hosts showed significant proliferation defects as measured by frequency and CellTrace Far Red dilution in cells that underwent proliferation in host spleens (Fig. 5, G and H, respectively). Considering the comparable BAFF (Fig. 5 B) and IL-7 (Fig. 5 E) concentrations in the serum of unirradiated *braum*^{-/-} mice and unirradiated WT littermates, the significant proliferation defect of WT naive B cells in *braum*^{-/-} hosts strongly suggests that the PDIA6 mutation impairs bioactivity of BAFF, IL-7 and perhaps other factors produced by the extra-hematopoietic compartment that contribute to the homeostasis of B cells.

We also examined protein abundance between *braum*^{-/-} and WT B cells, and tested if the changes can be regulated by the WT extra-hematopoietic environment by performing quantitative analyses of proteins using liquid chromatography with tandem mass spectrometry (LC-MS/MS). Among the 1,335 candidate proteins identified, 11 proteins implicated in immune cell development were reduced by 50% or more in *braum*^{-/-} B cells compared with those from WT littermates (Fig. 5 I and Data S1). We examined relative expression of seven of these proteins (BANK1, DOCK8, LYN, CDC42, STAT1, TAP1, and FoxP1) in *braum*^{-/-} B cells by immunoblot, which showed reductions of BANK, DOCK8, LYN, STAT1, and FoxP1 (Fig. S2). Next, we examined whether expression of these proteins could be rescued in B cells that developed in a PDIA6-competent extra-hematopoietic environment. We reconstituted irradiated *Rag2*^{-/-} recipients with WT or *braum*^{-/-} bone marrow cells and then isolated B cells for immunoblot analysis. We found that comparable levels of

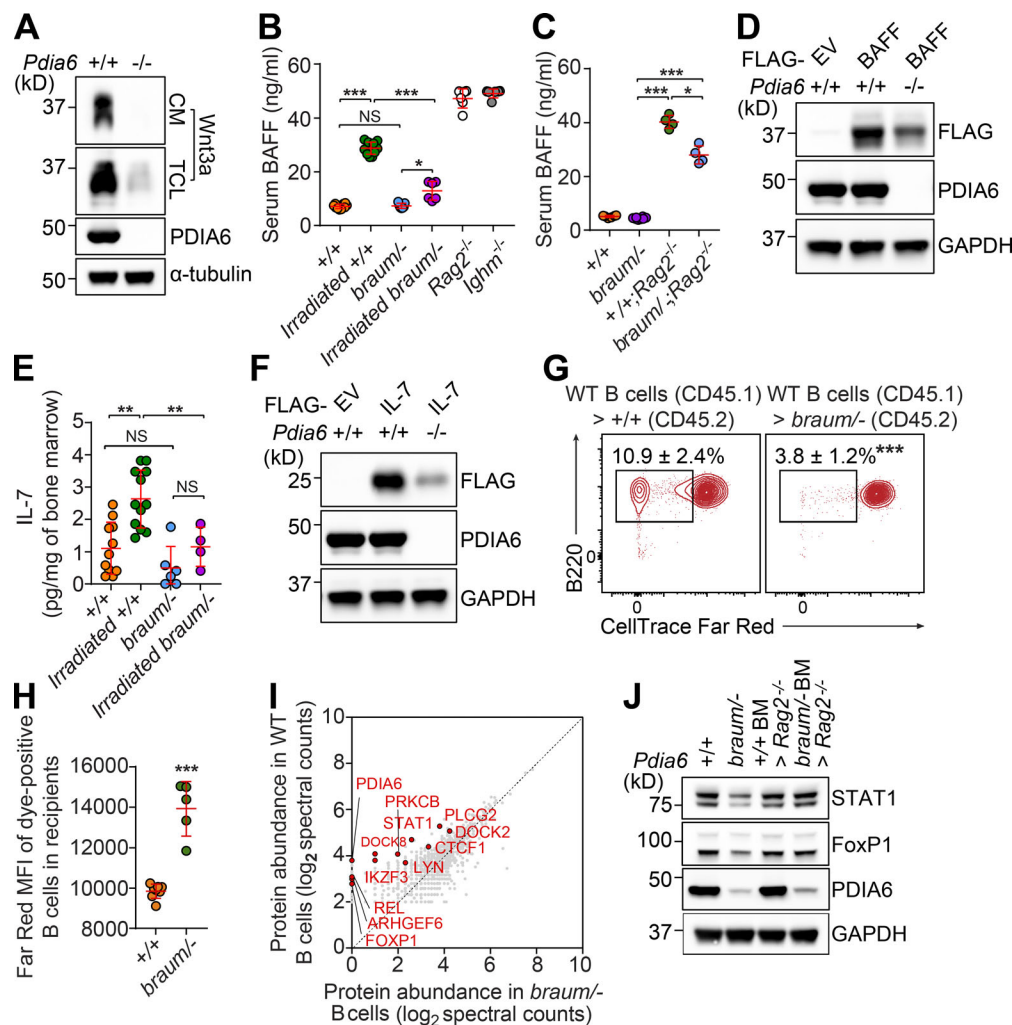


Figure 5. Impaired production of secreted signals by *Pdia6* mutant extra-hematopoietic cells. (A) Immunoblot analysis of Wnt3a in conditioned media (CM) and total cell lysates (TCL) of WT or *Pdia6*^{-/-} L-Wnt-3A fibroblasts generated by the CRISPR/Cas9 system. α -Tubulin was used as loading control. (B) Serum BAFF concentration in 12-wk-old *braum*^{-/-} and WT littermates before and 7 d after sublethal irradiation (8.5 Gy; *n* = 6–12 mice/group). Sera from 12-wk-old *Rag2*^{-/-} and *Ighm*^{-/-} mice were used as positive controls. (C) Serum BAFF concentration in 12-wk-old *braum*^{-/-}, *+/+*; *Rag2*^{-/-}, *braum*^{-/-}; *Rag2*^{-/-}, and WT littermates (*n* = 4–8 mice/genotype). (E) IL-7 level in bone marrow of unirradiated or sub-lethally irradiated (8.5 Gy) 8-wk-old *braum*^{-/-} and WT littermates (*n* = 4–12 mice/group). (D and F) Constructs encoding FLAG-tagged BAFF (D), or IL-7 (F) were transfected into *Pdia6*^{-/-} or parental L-Wnt3a cells. Total cell lysates were immunoblotted using the indicated antibodies. GAPDH was used as a loading control. (G and H) Impaired homeostatic expansion of WT B cells in *braum*^{-/-} mice. CellTrace Far Red-labeled WT naive B cells (CD45.1) were adoptively transferred into unirradiated *braum*^{-/-} or WT hosts (*n* = 5–8 mice/genotype). Frequency (G) and CellTrace Far Red dilution (H) were analyzed in the spleens of recipients 14 d after adoptive transfer. Numbers adjacent to outlined areas indicate percent cells in each (G). (I) Comparative analysis of protein abundance in splenic B cells isolated from *braum*^{-/-} and WT littermates identified by LC-MS/MS. (J) Immunoblot analysis of STAT1, FoxP1, and PDIA6 in lysates of B cells isolated from *braum*^{-/-} mice, WT littermates, and *Rag2*^{-/-} recipients engrafted with *braum*^{-/-} or WT bone marrow (*n* = 3–5 mice/group). GAPDH was used as loading control. Each symbol represents an individual mouse (B, C, E, and H). P values were determined by one-way ANOVA with Dunnett's multiple comparisons (B, C, and E) or Student's *t* test (H). Data are representative of one (I), two (E, G, H, and J), three (B and C), or five (A, D, and F) independent experiments. Error bars indicate SD. *, *P* < 0.05; **, *P* < 0.01; ***, *P* < 0.001; NS, not significant. EV, empty vector.

STAT1 and FoxP1 were expressed in *braum*^{-/-} or WT B cells repopulated in irradiated *Rag2*^{-/-} recipients (Fig. 5 J). This result suggests that the extra-hematopoietic function of PDIA6 is required for expression of multiple proteins that play critical roles in B cell survival and homeostasis.

Here we showed that deficiency of PDIA6 causes growth retardation, impaired insulin biosynthesis, and diabetes in mice. In addition, our findings demonstrate that PDIA6, operating in the extra-hematopoietic compartment, is necessary for lymphoid and myeloid development. We have shown evidence that

PDIA6 is needed for oxidative folding of proteins produced in the extra-hematopoietic compartment, such as Wnt3a, BAFF, and IL-7. We note that Peyer's patches and mesenteric lymph nodes were intact in adult *braum*^{-/-} mice, although other lymph nodes were smaller than those in WT mice; these findings indicate that *braum*^{-/-} mice are not completely devoid of IL-7 signaling during the fetal period. Moreover, this example supports the idea that a combined deficiency rather than the lack of a single factor is likely responsible for the phenotypes observed in *braum*^{-/-} mice. T cell-intrinsic PDIA6 function was also necessary to support the

expansion of *braum*^{-/-} T cells in response to homeostatic stimuli, in that *braum*^{-/-}-derived hematopoietic cells were at a mild disadvantage in repopulating thymocytes and peripheral T cells compared with WT cells in irradiated WT or *Rag2*^{-/-} recipients. Analysis of the *braum*^{-/-} T cell proteome should provide insight into the cell-intrinsic function of PDIA6 in T cell development and homeostasis. In view of the strong conservation between human and mouse PDIA6 orthologues (95% identity, Fig. S3) and the function of PDIA6 described in this study, we consider it likely that the same mechanism operates in humans. PDIA6 mutation may be considered as a possible etiology in unexplained syndromic immunodeficiency diseases in which severe diabetes is seen in the context of lymphoid and myeloid hypoplasia.

Materials and methods

Mice

8–10-wk-old pure C57BL/6J background males purchased from The Jackson Laboratory were mutagenized with ENU. Mutagenized G0 males were bred to C57BL/6J females, and the resulting G1 males were crossed to C57BL/6J females to produce G2 mice. G2 females were backcrossed to their G1 sires to yield G3 mice, which were screened for phenotypes. Whole-exome sequencing and mapping were performed as described previously (Wang et al., 2015). Heterozygous *Pdia6* knockout (*Pdia6*^{+/-}) mice were generated using the CRISPR/Cas9 system with *Pdia6* (5'-ACCGCTGACTGCTAGAAAGA-3') small base-pairing guide RNA (Ran et al., 2013). Compound heterozygous mice for the *braum* and null alleles (*braum*^{-/-}) were generated by breeding C57BL/6.SJL (CD45.1), *Rag2*^{-/-}, *Ighm*^{-/-}, and Tg(TcraTcrb)425Cbn (OT-II) transgenic mice were purchased from The Jackson Laboratory. All experiments in this study were approved by the University of Texas Southwestern Medical Center Institutional Animal Care and Use Committee.

Immunization

10-wk-old G3 or *braum*^{-/-} mice and WT littermates were immunized with OVA/alum (200 µg; Invivogen) on day 0 (i.m.) and the TI antigen NP₅₀-AECM-Ficoll (50 µg; Biosearch Technologies) on day 8 (i.p.) as previously described (Arnold et al., 2012). 6 d after NP₅₀-AECM-Ficoll immunization, blood was collected for ELISA.

For ELISA analysis of antigen-specific IgG and IgM responses, Nunc MaxiSorp flat-bottom 96-well microplates (Thermo Fisher Scientific) were coated with 5 µg/ml soluble OVA (Invivogen) or 5 µg/ml soluble NP8-BSA (Biosearch Technologies) and incubated at 4°C overnight. Plates were washed four times with washing buffer (0.05% [vol/vol] Tween-20 in PBS) using a BioTek microplate washer, then blocked with 1% (vol/vol) BSA in PBS for 1 h at room temperature. Serum samples were serially diluted in 1% (vol/vol) BSA, and then 1:50, 1:150, or dilutions described in the figures were added to the prepared ELISA plates. After a 2 h incubation, the plates were washed eight times with washing buffer and then incubated with HRP-conjugated goat anti-mouse IgG or IgM for 1 h at room temperature. Plates were washed eight times with washing buffer, then developed

with SureBlue TMB Microwell Peroxidase Substrate and TMB Stop Solution (KPL). Absorbance was measured at 450 nm on a Synergy Neo2 Plate Reader (BioTek). All ELISA data shown represent the 1:150 serum dilution or that indicated in the figure.

Bone marrow chimeras

Recipient mice were lethally irradiated with 13 Gy via gamma radiation (X-RAD 320, Precision X-Ray Inc.). The mice were given intravenous injection of 5 × 10⁶ bone marrow cells derived from the tibia and femurs of the donors. For 4 wk after engraftment, mice were maintained on antibiotics. 12 wk after bone marrow engraftment, the chimeras were immunized with NP-Ficoll as described above or euthanized to assess immune cell development in bone marrow, thymus, and spleen by flow cytometry. Chimerism was assessed using congenic CD45 markers.

Flow cytometry

Bone marrow cells, thymocytes, splenocytes, or peripheral blood cells were isolated, and RBC lysis buffer was added to remove the RBCs. Cells were stained at a 1:200 dilution with 15 mouse fluorochrome-conjugated monoclonal antibodies specific for the following murine cell surface markers encompassing the major immune lineages: B220, CD19, IgM, IgD, CD3ε, CD4, CD5, CD11c, CD44, CD43, CD25, CD21, CD23, BP-1 (BD PharMingen), CD8α, CD11b, NK1.1 (Biolegend), F4/80, and CD62L (Tonbo Biosciences), and in the presence of anti-mouse CD16/32 antibody (Tonbo Biosciences) for 1 h at 4°C. After staining, cells were washed twice in PBS and analyzed by flow cytometry. To stain the hematopoietic progenitor compartment, bone marrow was isolated and stained with Alexa Fluor 700-conjugated lineage markers (CD3, Ly-6G/6C, CD11b, B220, and Ter-119 at a 1:50 dilution; Biolegend), c-Kit, Sca-1, CD16/32, CD34, IL-7Rα (BD PharMingen), and CD135 (Biolegend) at a 1:100 dilution for 1 h at 4°C. After staining, cells were washed twice in PBS and analyzed by flow cytometry. Data were acquired on an LSRFortessa cell analyzer (BD Bioscience) and analyzed with FlowJo software (Treestar).

Blood/serum chemistries and ELISA

Mice were fasted for 6 h before glucose and insulin tolerance tests. Blood glucose was tested with the AlphaTRAK glucometer and test strips (Zoetis). The insulin tolerance test was initiated by i.p. injection with human insulin (0.75 U/kg; Sigma-Aldrich), and blood glucose was measured at set time points over the next 2 h (Zhang et al., 2016). ELISA kits were used to measure insulin, leptin, adiponectin (Crystal Chem), IGF1 (R&D Systems), triglyceride (Sigma-Aldrich), and BAFF (R&D Systems) in the serum according to the manufacturer's instructions. IL-7 was detected as described previously (Osborne et al., 2011). In brief, unirradiated or sublethally irradiated (8.5 Gy) mice were euthanized, and femurs were isolated 4 d after irradiation. Muscles, connective tissues, and condyles were removed by scissors. Each femur was placed in a 1.5-ml microcentrifuge tube and spun at 700 ×g, 4°C, for 3 min to isolate bone marrow. Bone marrow was resuspended in 100 µl PBS containing 1,000 U Collagenase IV (Sigma-Aldrich) and incubated at 55°C for

90 min. Cells were removed by centrifugation at 15,000 \times g, 4°C, for 10 min, and the supernatant was used directly for the IL-7 ELISA according to the manufacturer's instructions (R&D Systems).

Generation of PDIA6-deficient L-Wnt-3A cells

To generate the *Pdia6*^{-/-} L-Wnt-3A cell line (CRL-2647, ATCC), cells were transfected with PX458 plasmid encoding small base-pairing guide RNA targeting the genomic locus of mouse *Pdia6* (5'-ACCTTCTTTCTAGCAGTCAG-3'). 48 h after transfection, GFP⁺ cells were sorted by flow cytometry and single colonies selected by limiting dilution assay. The single colonies were screened and confirmed by immunoblot using a PDIA6 antibody (Proteintech).

In vivo T and B cell activation

Splenic CD45.1⁺ OT-II T cells were purified using the EasySep Mouse CD8⁺ T Cell Isolation Kit (StemCell Technologies). Purities were over 95% in all experiments as tested by flow cytometry. Cells were labeled with 5 μ M CellTrace Far Red (CD45.1⁺ OT-II), and equal numbers of labeled cells (2×10^6) were injected by the retro-orbital route into WT or *braum*^{-/-} (CD45.2⁺) mice. The next day, recipients were injected with either 100 μ g soluble OVA or sterile PBS as a control. Antigen (OVA)-specific T cell activation was analyzed based on the Far Red intensity of dividing OT-II cells after 72 h.

To assess the proliferative capacity of T cells in response to homeostatic proliferation signals, splenic pan T cells were isolated by using the mouse pan T cell isolation kit (StemCell Technologies). Isolated T cells from *braum*^{-/-} or WT littermates were stained with 5 μ M CellTrace Far Red. Equal numbers of stained cells (2×10^6) were transferred into *braum*^{-/-} or WT littermates that had been sublethally irradiated (8.5 Gy) 6 h earlier or into unirradiated controls. 7 d after adoptive transfer, splenocytes were prepared, surface-stained for CD3, CD4, and CD8, and then analyzed by flow cytometry for Far Red intensity.

To assess the proliferative capacity of B cells, splenic naive B cells (CD45.1) were isolated by using mouse CD43 MicroBeads (Miltenyi Biotec). Isolated cells were stained with 5 μ M CellTrace Far Red. Two million dye-labeled cells were transferred into *braum*^{-/-} or WT littermates that had been sublethally irradiated (8.5 Gy) 6 h earlier or into unirradiated controls (CD45.2). 14 d after adoptive transfer, splenocytes were prepared, surface-stained for CD45.1, CD45.2, CD3, and B220, and then analyzed by flow cytometry for Far Red intensity of dividing donor B cells.

Cell culture, transfection, and Western blot

HEK293T, *Pdia6*^{-/-}, or parental L-Wnt3A cells were grown at 37°C in DMEM (Life Technologies)/10% (vol/vol) FBS (Gibco)/1% antibiotics (Life Technologies) in 5% CO₂. Transfection of FLAG-tagged plasmids was performed using Lipofectamine 2000 (Life Technologies) according to the manufacturer's instructions. 36–48 h after transfection, cells were harvested in NP-40 lysis buffer (20 mM Tris-Cl, pH 7.5, 150 mM NaCl, 1 mM EDTA, 1 mM EGTA, 1% [vol/vol] NP-40, 2.5 mM sodium pyrophosphate, 1 mM β -glycerophosphate, 1 mM Na₃VO₄, and protease inhibitors) for 45 min at 4°C. Whole-cell lysates were analyzed using anti-FLAG

M2 antibody (Sigma-Aldrich) using standard procedures for Western blot analysis as described below.

For direct Western blot analysis, cells were lysed in 1% (wt/vol) SDS (Thermo Fisher Scientific), 0.01% (wt/vol) Benzonase (Sigma-Aldrich), and protease inhibitor cocktail (Cell Signaling Technology) in buffer A (50 mM HEPES, 2 mM MgCl₂, and 10 mM KCl). Protein concentration was measured using a bicinchoninic acid assay (Pierce). 10 μ g of protein was separated on 4–12% Bis-Tris protein gels (Life Technologies), and proteins were transferred to nitrocellulose membranes (Bio-Rad) for 45 min at 13 V. After blocking in Tris-buffered saline containing 0.05% (vol/vol) Tween-20 with 5% (wt/vol) nonfat dry milk at room temperature for 1 h, the membrane was incubated overnight with primary antibodies anti-insulin, anti-Pdia6, anti-STAT1, anti-FoxP1, anti-Wnt3a, anti- α -tubulin, or anti-GAPDH (Cell Signaling Technology) at 4°C in 5% (wt/vol) nonfat dry milk in Tris-buffered saline containing 0.05% (vol/vol) Tween-20 with gentle rocking. The membrane was then incubated with secondary antibody goat anti-rabbit or mouse IgG-HRP (Thermo Fisher Scientific) for 1 h at room temperature with gentle rocking. The chemiluminescence signal was developed using the SuperSignal West Dura Extended Duration Substrate kit (Thermo Fisher Scientific) and detected by a G:Box Chemi XX6 system (Syngene).

PDI activity measurement

FLAG-tagged WT and mutant PDIA6 were produced in HEK293T cells by transient transfection of plasmids as described above and purified with anti-FLAG M2 agarose beads (Sigma-Aldrich). The PROTEOSTAT PDI assay kit (Enzo Life Sciences) was used to measure catalytic reduction of insulin by purified PDIA6 proteins according to the manufacturer's instructions. Briefly, WT PDIA6 or mutant PDIA6 was added to insulin. Then, dithiothreitol was added to start PDI reduction activity. The reaction was stopped by the Stop reagent, and the insulin precipitate was fluorescently labeled with Proteostat PDI detection reagent for 15 min. Fluorescence intensity was measured at 500 nm excitation and 603 nm emission using a Synergy Neo2 Plate Reader (BioTek).

Statistical analysis

The statistical significance of differences between groups was analyzed using GraphPad by performing the indicated statistical tests. Differences in the raw values among groups were considered statistically significant when $P < 0.05$. P values are denoted by *, $P < 0.05$; **, $P < 0.01$; ***, $P < 0.001$; ns, not significant with $P > 0.05$.

Online supplemental material

Fig. S1 shows impaired antigen-specific expansion of WT OT-II T cells in *braum*^{-/-} mice. Fig. S2 shows immunoblot analysis of key immune system proteins, initially identified as differentially expressed by LC-MS/MS, in B cells isolated from *braum*^{-/-} and WT littermates. Fig. S3 shows amino acid sequence alignment of human and mouse PDIA6. Data S1 contains the list of proteins identified by quantitative LC-MS/MS analysis of *braum*^{-/-} and WT B cell lysates.

Acknowledgments

This work was supported by a grant from the National Institutes of Health (R01-AI125581) and by the Lyda Hill Foundation. J.H. Choi, X. Zhan, J. Russell, S. Ludwig, X. Li, M. Tang, P. Anderton, and B. Beutler received salary support from Pfizer.

Author contributions: Conceptualization: J.H. Choi, B. Beutler; formal analysis: J.H. Choi, X. Zhong, B. Beutler; funding acquisition: B. Beutler; investigation: J.H. Choi, X. Zhong, Z. Zhang, W. McAlpine, T.C. Liao, T. Misawa, B. Beutler; methodology: J.H. Choi, X. Zhong, L. Su, B. Beutler; project administration: J.H. Choi, B. Beutler; resources: J.H. Choi, X. Zhong, X. Zhan, X. Li, M. Tang, P. Anderton, J. Russell, S. Ludwig, B. Beutler; supervision: B. Beutler; validation: J.H. Choi, X. Zhong; visualization: J.H. Choi; writing (original draft): J.H. Choi; writing (review and editing): J.H. Choi, E.M.Y. Moresco, B. Beutler.

Disclosures: The authors declare no competing interests exist.

Submitted: 2 January 2019

Revised: 6 June 2019

Accepted: 20 December 2019

References

- Adzhubei, I.A., S. Schmidt, L. Peshkin, V.E. Ramensky, A. Gerasimova, P. Bork, A.S. Kondrashov, and S.R. Sunyaev. 2010. A method and server for predicting damaging missense mutations. *Nat. Methods*. 7:248–249. <https://doi.org/10.1038/nmeth0410-248>
- Anthony, B.A., and D.C. Link. 2014. Regulation of hematopoietic stem cells by bone marrow stromal cells. *Trends Immunol.* 35:32–37. <https://doi.org/10.1016/j.it.2013.10.002>
- Arnold, C.N., E. Pirie, P. Dosenovic, G.M. McInerney, Y. Xia, N. Wang, X. Li, O.M. Siggs, G.B. Karlsson Hedestam, and B. Beutler. 2012. A forward genetic screen reveals roles for Nfkb1d, Zeb1, and Ruvbl2 in humoral immunity. *Proc. Natl. Acad. Sci. USA*. 109:12286–12293. <https://doi.org/10.1073/pnas.1209134109>
- Chen, G., S. Peng, M. Zou, H. Xu, D. Xu, and J. Wang. 2004. Construction and function of two Cys146-mutants with high activity, derived from recombinant human soluble B lymphocyte stimulator. *J. Biochem.* 136: 73–79. <https://doi.org/10.1093/jb/mvh088>
- Corfe, S.A., and C.J. Paige. 2012. The many roles of IL-7 in B cell development; mediator of survival, proliferation and differentiation. *Semin. Immunol.* 24:198–208. <https://doi.org/10.1016/j.smim.2012.02.001>
- Cosenza, L., E. Sweeney, and J.R. Murphy. 1997. Disulfide bond assignment in human interleukin-7 by matrix-assisted laser desorption/ionization mass spectroscopy and site-directed cysteine to serine mutational analysis. *J. Biol. Chem.* 272:32995–33000. <https://doi.org/10.1074/jbc.272.52.32995>
- Eletto, D., D. Eletto, D. Dersh, T. Gidalevitz, and Y. Argon. 2014. Protein disulfide isomerase A6 controls the decay of IRE1α signaling via disulfide-dependent association. *Mol. Cell.* 53:562–576. <https://doi.org/10.1016/j.molcel.2014.01.004>
- Eletto, D., D. Eletto, S. Boyle, and Y. Argon. 2016. PDIA6 regulates insulin secretion by selectively inhibiting the RIDD activity of IRE1. *FASEB J.* 30: 653–665. <https://doi.org/10.1096/fj.15-275883>
- Ernst, B., D.S. Lee, J.M. Chang, J. Sprent, and C.D. Surh. 1999. The peptide ligands mediating positive selection in the thymus control T cell survival and homeostatic proliferation in the periphery. *Immunity*. 11: 173–181. [https://doi.org/10.1016/S1074-7613\(00\)80092-8](https://doi.org/10.1016/S1074-7613(00)80092-8)
- Fehniger, T.A., and M.A. Caligiuri. 2001. Interleukin 15: biology and relevance to human disease. *Blood*. 97:14–32. <https://doi.org/10.1182/blood.V97.1.14>
- Gorasia, D.G., N.L. Dudek, H. Safavi-Hemami, R.A. Perez, R.B. Schittenhelm, P.M. Saunders, S. Wee, J.E. Mangum, M.J. Hubbard, and A.W. Purcell. 2016. A prominent role of PDIA6 in processing of misfolded proinsulin. *Biochim. Biophys. Acta*. 1864:715–723. <https://doi.org/10.1016/j.bbapap.2016.03.002>
- Gorelik, L., K. Gilbride, M. Dobles, S.L. Kalled, D. Zandman, and M.L. Scott. 2003. Normal B cell homeostasis requires B cell activation factor

- production by radiation-resistant cells. *J. Exp. Med.* 198:937–945. <https://doi.org/10.1084/jem.20030789>
- Hara, T., S. Shitara, K. Imai, H. Miyachi, S. Kitano, H. Yao, S. Tani-ichi, and K. Ikuta. 2012. Identification of IL-7-producing cells in primary and secondary lymphoid organs using IL-7-GFP knock-in mice. *J. Immunol.* 189: 1577–1584. <https://doi.org/10.4049/jimmunol.1200586>
- Henney, C.S. 1989. Interleukin 7: effects on early events in lymphopoiesis. *Immunol. Today*. 10:170–173. [https://doi.org/10.1016/0167-5699\(89\)90175-8](https://doi.org/10.1016/0167-5699(89)90175-8)
- Jordan, P.A., J.M. Stevens, G.P. Hubbard, N.E. Barrett, T. Sage, K.S. Authi, and J.M. Gibbins. 2005. A role for the thiol isomerase protein ERP5 in platelet function. *Blood*. 105:1500–1507. <https://doi.org/10.1182/blood-2004-02-0608>
- Karpusas, M., T.G. Cachero, F. Qian, A. Boriack-Sjodin, C. Mullen, K. Strauch, Y.M. Hsu, and S.L. Kalled. 2002. Crystal structure of extracellular human BAFF, a TNF family member that stimulates B lymphocytes. *J. Mol. Biol.* 315:1145–1154. <https://doi.org/10.1006/jmbi.2001.5296>
- Kikuchi, M., E. Doi, I. Tsujimoto, T. Horibe, and Y. Tsujimoto. 2002. Functional analysis of human P5, a protein disulfide isomerase homologue. *J. Biochem.* 132:451–455. <https://doi.org/10.1093/oxfordjournals.jbchem.a003242>
- Kraus, M., M.B. Alimzhanov, N. Rajewsky, and K. Rajewsky. 2004. Survival of resting mature B lymphocytes depends on BCR signaling via the Igα/Igβ heterodimer. *Cell*. 117:787–800. <https://doi.org/10.1016/j.cell.2004.05.014>
- Laurindo, F.R., L.A. Pescatore, and D.C. Fernandes. 2012. Protein disulfide isomerase in redox cell signaling and homeostasis. *Free Radic. Biol. Med.* 52:1954–1969. <https://doi.org/10.1016/j.freeradbiomed.2012.02.037>
- Lee, Y., M. Decker, H. Lee, and L. Ding. 2017. Extrinsic regulation of hematopoietic stem cells in development, homeostasis and diseases. *Wiley Interdiscip. Rev. Dev. Biol.* 6:e279. <https://doi.org/10.1002/wdev.279>
- MacDonald, B.T., A. Hien, X. Zhang, O. Iranloye, D.M. Virshup, M.L. Waterman, and X. He. 2014. Disulfide bond requirements for active Wnt ligands. *J. Biol. Chem.* 289:18122–18136. <https://doi.org/10.1074/jbc.M114.575027>
- Mackay, F., P. Schneider, P. Rennert, and J. Browning. 2003. BAFF AND APRIL: a tutorial on B cell survival. *Annu. Rev. Immunol.* 21:231–264. <https://doi.org/10.1146/annurev.immunol.21.120601.141152>
- Makino, S., K. Kunimoto, Y. Muraoka, Y. Mizushima, K. Katagiri, and Y. Tochino. 1980. Breeding of a non-obese, diabetic strain of mice. *Jikken Dobutsu*. 29:1–13.
- Osawa, M., K. Hanada, H. Hamada, and H. Nakauchi. 1996. Long-term lymphohematopoietic reconstitution by a single CD34-low/negative hematopoietic stem cell. *Science*. 273:242–245. <https://doi.org/10.1126/science.273.5272.242>
- Osborne, L.C., D.T. Patton, J.H. Seo, and N. Abraham. 2011. Elevated IL-7 availability does not account for T cell proliferation in moderate lymphopenia. *J. Immunol.* 186:1981–1988. <https://doi.org/10.4049/jimmunol.1002224>
- Passam, F.H., L. Lin, S. Gopal, J.D. Stopa, L. Bellido-Martin, M. Huang, B.C. Furie, and B. Furie. 2015. Both platelet- and endothelial cell-derived ERp5 support thrombus formation in a laser-induced mouse model of thrombosis. *Blood*. 125:2276–2285. <https://doi.org/10.1182/blood-2013-12-547208>
- Ran, F.A., P.D. Hsu, J. Wright, V. Agarwala, D.A. Scott, and F. Zhang. 2013. Genome engineering using the CRISPR-Cas9 system. *Nat. Protoc.* 8: 2281–2308. <https://doi.org/10.1038/nprot.2013.143>
- Reya, T., A.W. Duncan, L. Ailles, J. Domen, D.C. Scherer, K. Willert, L. Hintz, R. Nusse, and L.L. Weissman. 2003. A role for Wnt signalling in self-renewal of haematopoietic stem cells. *Nature*. 423:409–414. <https://doi.org/10.1038/nature01593>
- Sawai, C.M., S. Babovic, S. Upadhaya, D.J.H.F. Knapp, Y. Lavin, C.M. Lau, A. Goloborodko, J. Feng, J. Fujisaki, L. Ding, et al. 2016. Hematopoietic Stem Cells Are the Major Source of Multilineage Hematopoiesis in Adult Animals. *Immunity*. 45:597–609. <https://doi.org/10.1016/j.immuni.2016.08.007>
- Sugimura, R., X.C. He, A. Venkatraman, F. Arai, A. Box, C. Semerad, J.S. Haug, L. Peng, X.B. Zhong, T. Suda, and L. Li. 2012. Noncanonical Wnt signaling maintains hematopoietic stem cells in the niche. *Cell*. 150: 351–365. <https://doi.org/10.1016/j.cell.2012.05.041>
- Tan, J.T., E. Dudl, E. LeRoy, R. Murray, J. Sprent, K.I. Weinberg, and C.D. Surh. 2001. IL-7 is critical for homeostatic proliferation and survival of naive T cells. *Proc. Natl. Acad. Sci. USA*. 98:8732–8737. <https://doi.org/10.1073/pnas.161126098>
- Wang, T., X. Zhan, C.H. Bu, S. Lyon, D. Pratt, S. Hildebrand, J.H. Choi, Z. Zhang, M. Zeng, K.W. Wang, et al. 2015. Real-time resolution of point mutations that cause phenovariance in mice. *Proc. Natl. Acad. Sci. USA*. 112:E440–E449. <https://doi.org/10.1073/pnas.1423216112>
- Zhang, Z., E. Turer, X. Li, X. Zhan, M. Choi, M. Tang, A. Press, S.R. Smith, A. Divoux, E.M. Moresco, and B. Beutler. 2016. Insulin resistance and diabetes caused by genetic or diet-induced KBTBD2 deficiency in mice. *Proc. Natl. Acad. Sci. USA*. 113:E6418–E6426. <https://doi.org/10.1073/pnas.1614467113>

Supplemental material

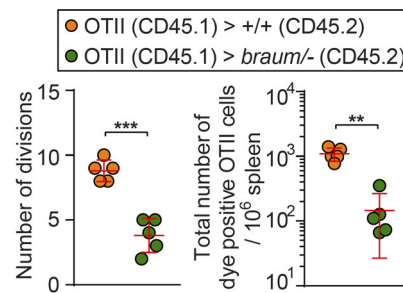


Figure S1. **Impaired antigen-specific expansion of WT OT-II T cells in *braum*^{-/-} mice.** Number of divisions (left) and quantification of total numbers (right) of CellTrace Far Red-labeled WT OT-II cells harvested from *braum*^{-/-} and WT littermates 72 h after injection of soluble OVA. Data points represent individual mice. P values were determined by Student's *t* test. Data are representative of two independent experiments with five mice per genotype. Error bars indicate SD. **, *P* < 0.01; ***, *P* < 0.001.

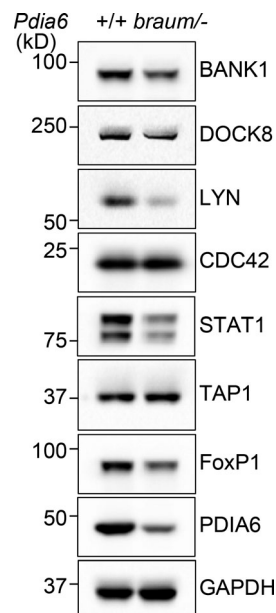


Figure S2. **Confirmation of expression levels of proteins identified by quantitative LC-MS/MS analysis.** Immunoblot analysis of BANK1, DOCK8, LYN, CDC42, STAT1, TAP1, FoxP1, PDIA6, and GAPDH in total cell lysates of pooled splenic B cells from 12-wk-old *braum*^{-/-} or WT littermates. Data are representative of three independent experiments.

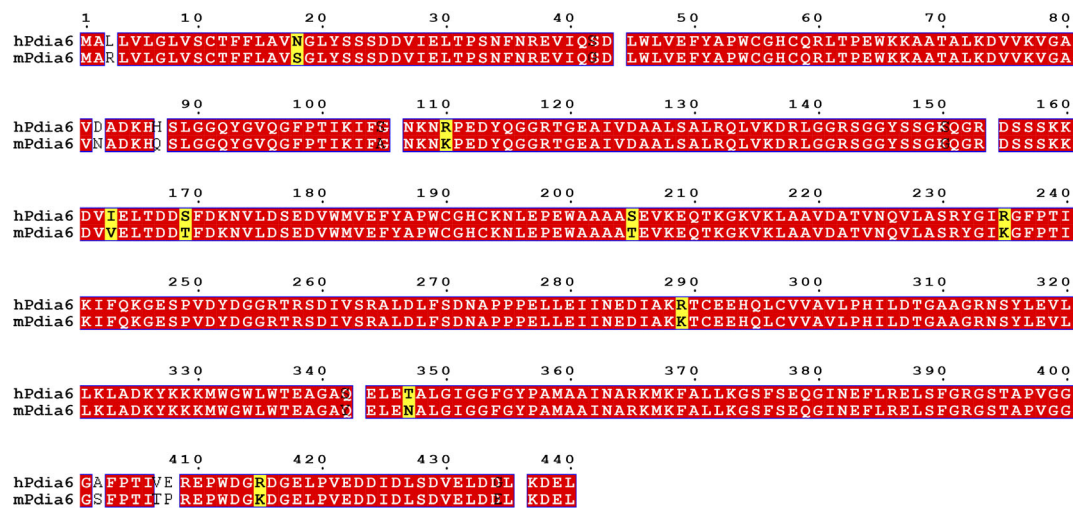


Figure S3. **Amino acid sequence alignment of human and mouse PDIA6.** Identical residues are highlighted in red, and similar residues are highlighted in yellow. GenBank gene accession no. for human PDIA6 is NP_001269633.1, and mouse PDIA6 is NP_082235.1.

A supplemental dataset is provided online that shows the abundance of proteins in B cells isolated from *braun*^{-/-} or WT littermates identified by LC-MS/MS analysis.